



The Relation Between Barrier Structure and Current Uniformity in YBCO Josephson Junctions

M. CARMODY*, K.L. MERKLE AND Y. HUANG[†]

*Materials Science Division and Science and Technology Center for Superconductivity,
Argonne National Laboratory, Argonne, Illinois 60439, USA*
carmody@anl.gov

L.D. MARKS

Materials Science and Engineering Department, Northwestern University, Evanston Illinois 60208, USA

B.H. MOECKLY

Conductus, Inc. 969 West Maude Ave. Sunnyvale, CA 94086, USA

Abstract. Electromagnetic transport measurements were combined with high-resolution electron microscopy observations to study the relation between structure and local critical currents in $\text{YBa}_2\text{Cu}_3\text{O}_{7-x}$ (YBCO) Josephson junctions. The spatial variation of the critical current $J(x)$ along the length of the boundary for interface engineered Josephson junctions and bicrystal grain boundary Josephson junctions was determined using a phase retrieval algorithm. The current distribution solutions were found to be highly uniform along the length of interface engineered junctions in contrast to solutions for grain boundary junctions. The latter showed significant spatial oscillations in the critical current as well as areas along the boundary that carried no current. Microstructural evaluation of interface engineered junctions fabricated using identical processing parameters to the junctions used for transport measurements suggest that the uniform current distribution is controlled by a highly uniform barrier layer formed between the superconducting electrodes. Microstructural evaluation of grain boundary junctions similar to the junctions used for transport measurements show considerable variations of the grain boundary structure within a single junction.

Keywords: Josephson junctions, HREM, current distribution, grain boundaries

1. Introduction

High T_c Josephson junctions have shown large scatter in their transport properties. The vast scatter in the transport properties found in the various types of Josephson junctions can be largely attributed to the variation of the interface barrier structure from one junction to another. Understanding how the microstructure of the interface for a Josephson junction correlates to the current crossing the interface will result in an improved

understanding of the mechanisms controlling the transport processes.

One promising type of Josephson junction for device applications are the ramp-edge type Josephson junctions. The microstructure of the interface between the superconducting electrodes in these junctions can play an important role in determining the uniformity of the junction transport properties and thus the junctions potential usefulness for device applications. It is believed that the structural uniformity of the barrier layer is directly related to the current crossing the boundary and therefore determines the reproducibility of these junctions [1–14]. There are many factors that can influence

*To whom all correspondence should be addressed.

[†]Present address: Navistar Corp., Melrose Park, IL, USA.

the uniformity of the barrier layer and thus the current distribution across the boundary. Local oxygen content variation, boundary precipitates, interfacial strain fields and boundary microstructure can all play an important role [1–14].

Previous work on plasma treated and ion milled YBCO surfaces has shown that these treatments result in structural changes to the YBCO. These treated YBCO surfaces can act as a Josephson barrier. Understanding that the interface layer can play a dominant role in controlling the reproducibility in manufacturing Josephson junctions, Moeckly and Char developed a method for fabricating ramp-edge Josephson junctions without the growth of a heterophase interlayer [15, 16]. Instead, they applied an Ar/O plasma treatment to the surface of the first $\text{YBa}_2\text{Cu}_3\text{O}_{7-x}$ (YBCO) layer in the ramp edge junction forming an intermediate layer which acts as a Josephson junction barrier. These interface engineered junctions have been shown to be highly reproducible with resistively-shunted junction like I-V characteristics, Fraunhofer like magnetic field response and $I_c R_n$ values between 0.1–0.5 mV [15, 16].

To gain a better understanding of the properties as they relate to the reproducibility of the interface engineered junctions, we have studied the current distribution across both ramp-edge and grain boundary YBCO Josephson junctions. Understanding how the current distribution across the boundary varies from one type of junction to another and how that variation correlates to the boundary microstructure will provide insight to the mechanism controlling the transport process across the boundary. Calculations of the critical current variations along the length of the boundary were performed, based on critical current vs. applied magnetic field measurements. Critical current vs. applied magnetic field measurements on YBCO interface engineered ramp-edge junctions and 24° bicrystal grain boundary junctions were performed with the magnetic field applied perpendicular to the substrate surface. The current distribution along the length of the boundary (as defined in Fig. 1) for each sample was calculated using a phase retrieval algorithm [17, 18]. Details of the critical current distribution $J(x)$ calculations have been reported previously [17, 18]. The possibility of multiple solutions has been accounted for and when multiple

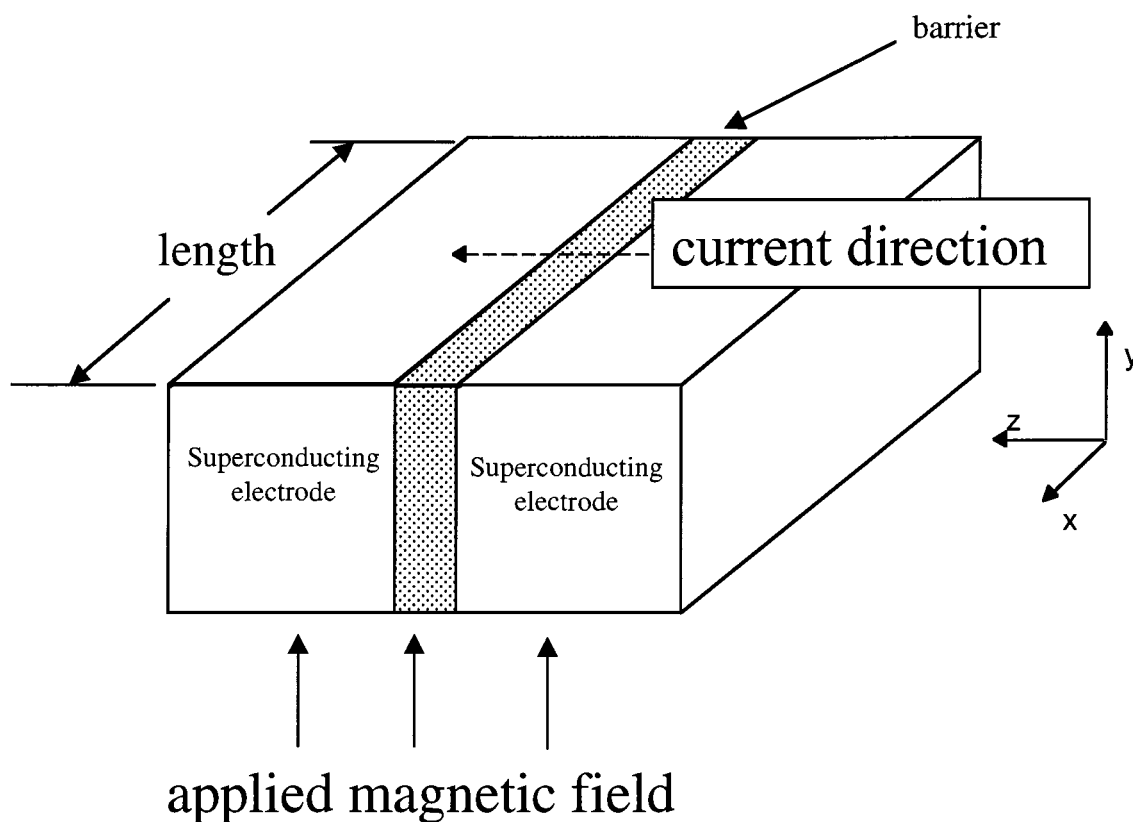


Figure 1. Schematic of the basic superconductor-barrier-superconductor geometry considered for boundary transport measurements and analysis. The magnetic field is applied perpendicular to both the current bias direction and the length of the boundary.

solutions were found, all solutions were considered to be possible correct current distributions [17, 18].

High resolution electron microscopy was performed on both YBCO interface engineered junctions and 24° YBCO grain boundary Josephson junctions. The junctions used for microstructural analysis were fabricated using similar processing parameters to the junctions used for transport analysis. The microstructure of each boundary type was compared to the current variations determined from the critical current vs. applied magnetic field measurements. By understanding how the current distribution changes along the boundary it is possible to relate the microstructure to the current transport across the boundary and thus gain insight into mechanism controlling the process.

2. Results

A. Current Distributions

Transport measurements were performed on grain boundary and interface engineered junctions to analyze the distribution of the current along the length

of the boundary. The total critical current across the boundary as a function of an applied magnetic flux ($I_c(B)$) was measured for a 24° YBCO grain boundary Josephson junction, grown epitaxially on a 24° [001] symmetric SrTiO₃ bicrystal substrate. Figure 2 shows a critical current vs. applied magnetic field measurement of a 24° YBCO grain boundary junction measured at 4.2 Kelvin.

The critical current as a function of an applied magnetic field $I_c(B)$ can be written as the Fourier transform of the positional current density distribution $J(x)$. Specifically,

$$I_c(B) = \left| \int_0^L J(x) \exp(i\phi(x)) dx \right|, \quad (1)$$

where $\phi(x) = qx + \phi_0$ and $q = 2\pi DB/\Phi_0$ (B is the magnetic flux perpendicular to the current direction, Φ_0 is defined as the superconducting flux quantum ($h/2e = 2.07 \times 10^{-7}$ G cm²) and $D = \lambda_1 + \lambda_2 + d$ where d is the thickness of the barrier and λ the London penetration depth. Using the Fourier relation from Eq. (1) it is possible to invert $I_c(B)$ using a phase retrieval algorithm and obtain the positional current distribution $J(x)$ [17].

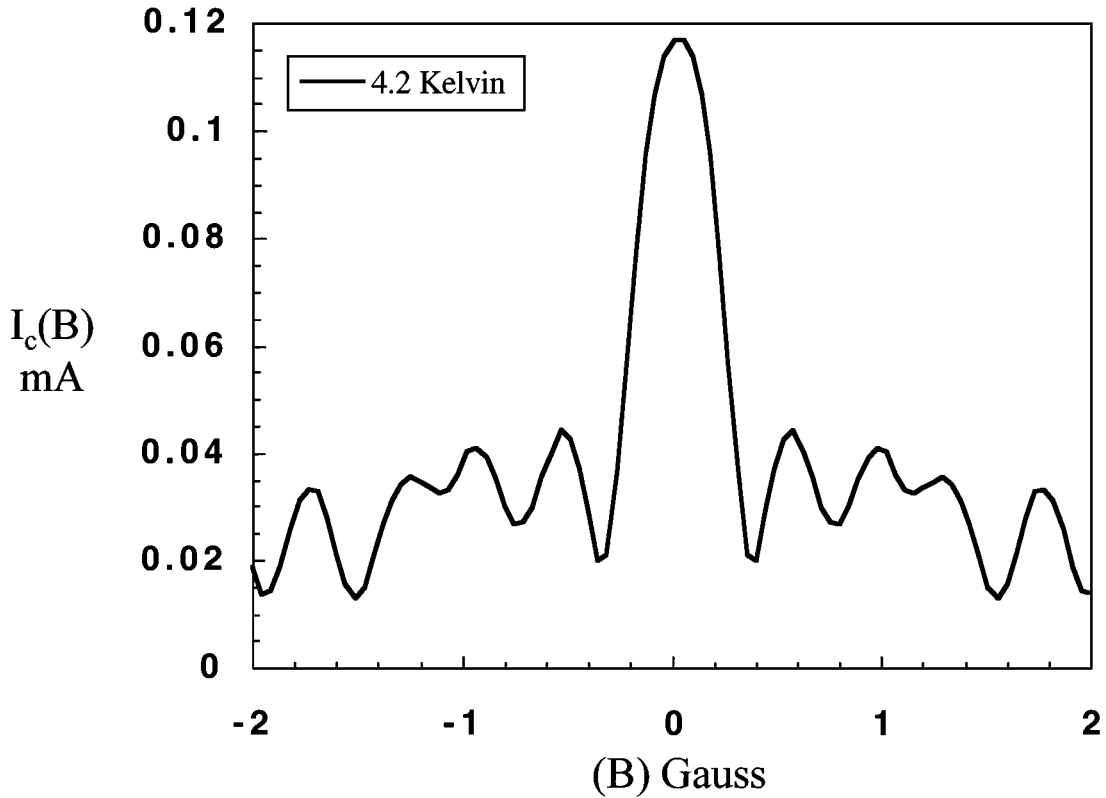


Figure 2. Critical current vs. applied magnetic field measurements for a typical 24° YBCO grain boundary junction measured at 4.2 Kelvin.

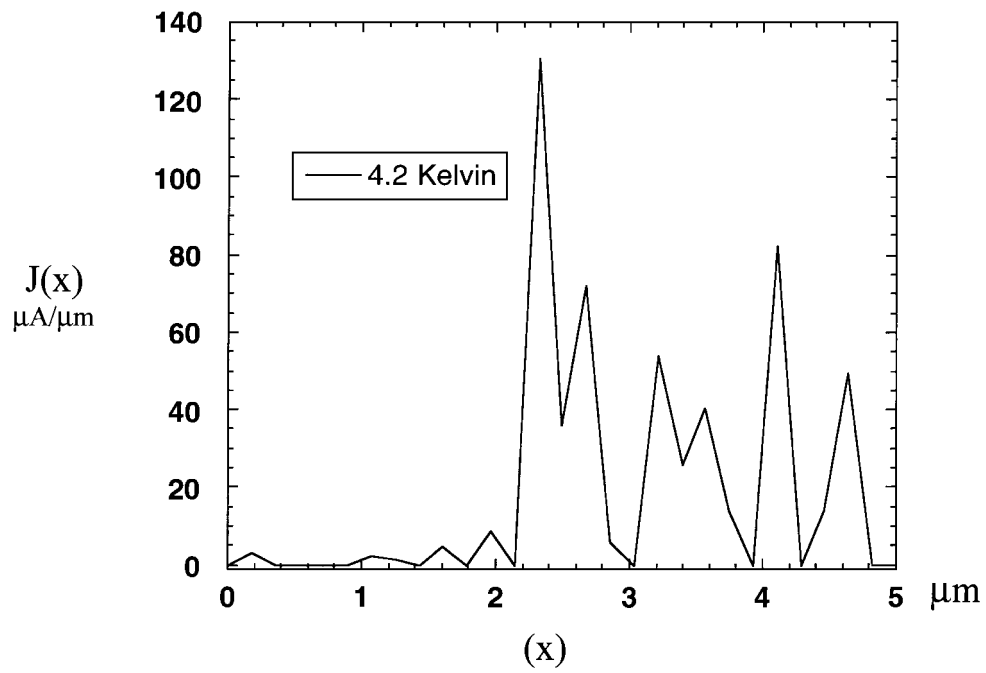


Figure 3. Current distribution $J(x)$ along the length of a grain boundary junction calculated from the critical current vs. applied magnetic field measurements in Fig. 4.

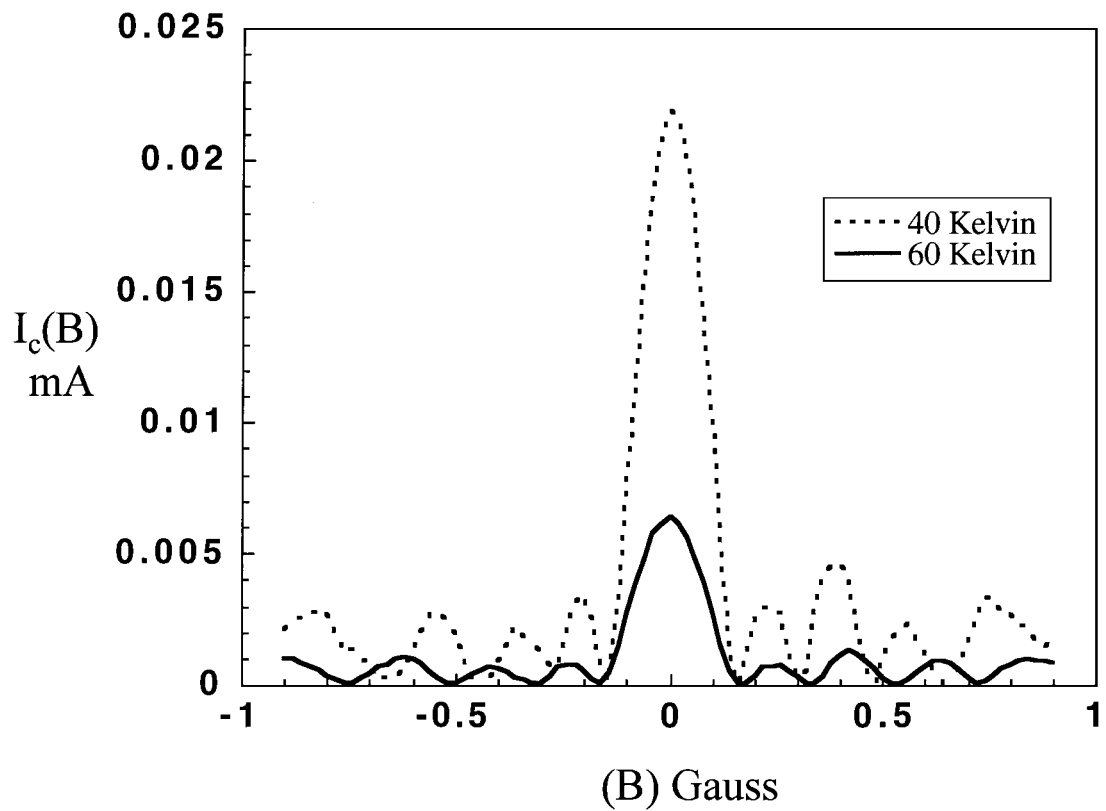


Figure 4. Critical current vs. applied magnetic field measurements for and interface engineered ramp-edge junction measured at 40 Kelvin and 60 Kelvin.

Figure 3 presents the positional current distribution ($J(x)$ from Eq. (1)) determined from the data in Fig. 2 using the previously mentioned phase retrieval algorithm. Note the extreme variations in the critical current along the boundary as well as a region along the boundary that carries practically zero current.

Critical current vs. applied magnetic field measurements were performed on an interface engineered junction for analysis of the current distribution. Figure 4 depicts the critical current vs. applied magnetic field for a typical interface engineered junction. Measurements were performed at 40 Kelvin and 60 Kelvin. Figure 5 shows the critical current distributions $J(x)$ along the length of the boundary for each measured temperature from the sample in Fig. 4. Note that the magnetic field dependence of the sample in Fig. 4 shows only minor deviations from the ideal Fraunhofer pattern and therefore results in a fairly uniform current distribution along the length of the boundary in Fig. 5.

B. Boundary Microstructure

The microstructure of the grain boundary for a 24° Josephson junction was analyzed using high resolution electron microscopy (HREM). Thus, combining results from the electromagnetic junction characterization with microstructure observations allows us to correlate the variations of the transport properties to the boundary microstructure.

Figure 6 is an HREM image of a small section of the 24° YBCO grain boundary junction. The length of the boundary shown in Fig. 6 is relatively straight and the grain boundary plane is near a symmetric orientation. However, we note that this boundary region is inclined at approximately 45° relative to the bicrystal grain boundary of the underlying substrate. The grain boundary core appears disordered in a region less than a nanometer in width. Figure 7 shows an HREM image of a different region along the same YBCO grain

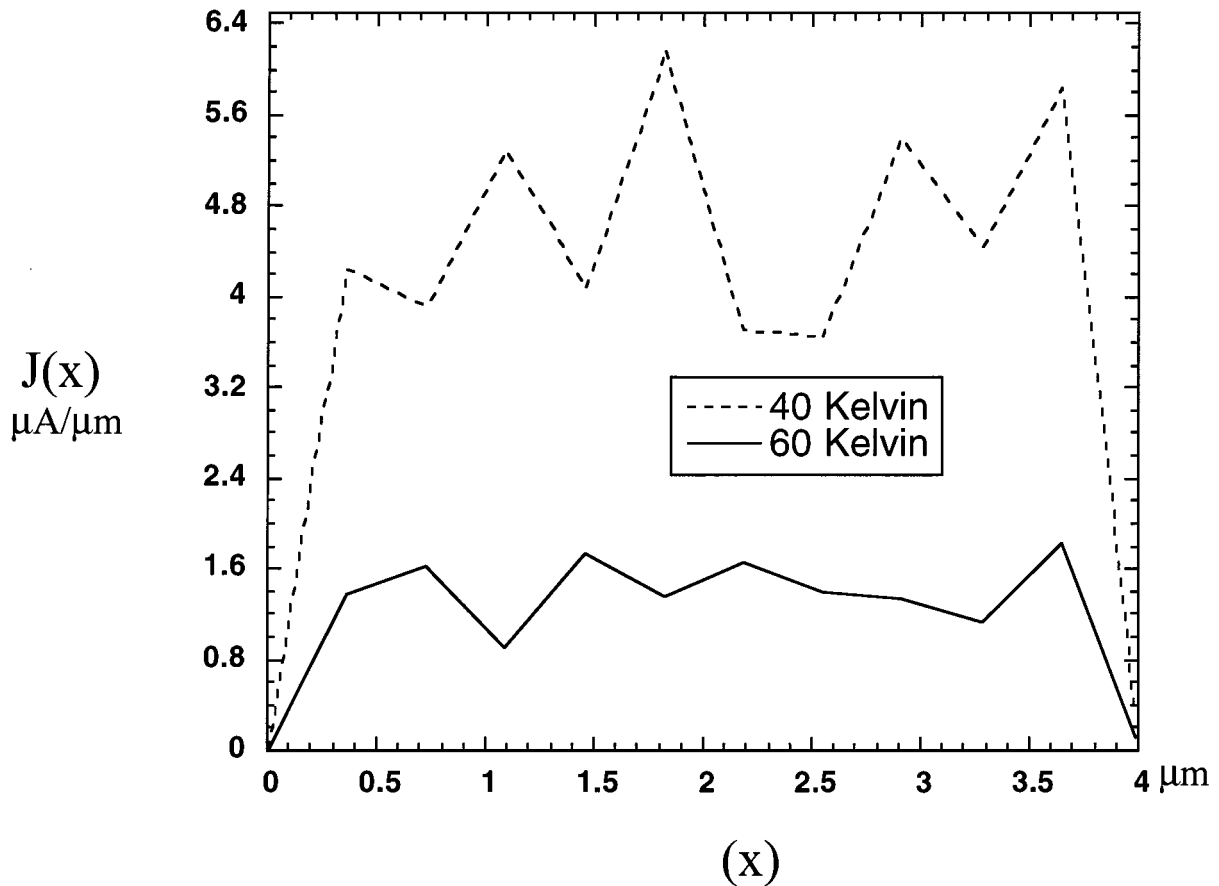


Figure 5. Current distribution $J(x)$ along the length of an interface engineered junction boundary calculated from the measurements in Fig. 1.

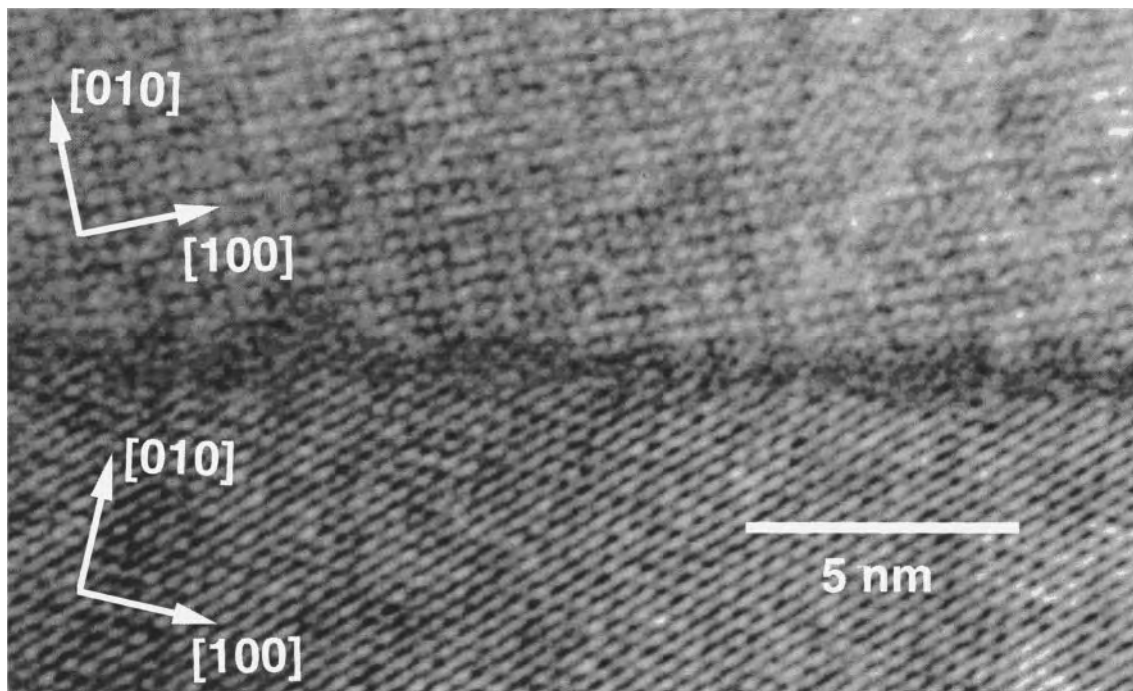


Figure 6. HREM image of a [001], 24° YBCO grain boundary junction grown on a [001] symmetric 24° SrTiO₃ bicrystal template. Note that this area of the boundary is relatively straight and has a disordered region at the boundary.

boundary. Here the grain boundary is inclined relative to the film normal but largely parallel to [010] of the top crystal. The appearance of asymmetric facets is typical of large regions of the grain boundary. The Morié, pattern in Fig. 7 evident at the boundary is indicative of an incline and overlapping of the two crystals in the direction of the electron beam. The HREM image of Fig. 8 depicts another asymmetric region of the same grain boundary. Again, the large width of the Morié, pattern at the grain boundary indicates considerable crystal overlap due to the inclined grain boundary plane. Figure 9 shows an HREM image of an asymmetric section of the same grain boundary. Within this grain boundary section the grain boundary is largely parallel to the electron beam direction, but some variation in the grain boundary inclination is evident. This last grain boundary appears to contain core regions that are well connected. Grains that are well connected, in contrast to cores that are strongly disordered, such as is Fig. 6, are expected to carry higher critical currents. Figures 6–9 demonstrate the great variation in the local microstructure of grain boundaries, which is to a large extent due to the grain boundary meandering, as discussed below.

High resolution electron microscopy was also used to image the barrier layer of an interface engineered junction for comparison of the boundary microstructure with the boundary transport properties. Figure 10 is a HREM image of a typical interface engineered ramp-edge junction. The image shows a fairly uniform boundary layer approximately 1–2 nm wide. The interface layer is continuous and free of pinholes and secondary phases which would act to disrupt the uniformity of the current flow. Only small steps along the barrier layer are evident with no significant strain effects visible. Huang and co-workers have confirmed that the boundary layer of the interface engineered junctions are crystalline with a different structure than the bulk YBCO [19]. Since the planes of the interface engineered junctions, as in Fig. 10 are typically not exactly parallel to the zone axis, a test sample was prepared by introducing the interface engineered barrier layer on the YBCO basal plane. An HREM image of this is shown in Fig. 11, where the first YBCO layer was plasma treated without the formation of a ramp surface. The resulting fringes of the barrier layer indicate a well structured boundary layer with a structure distinctly different from the two superconducting layers.

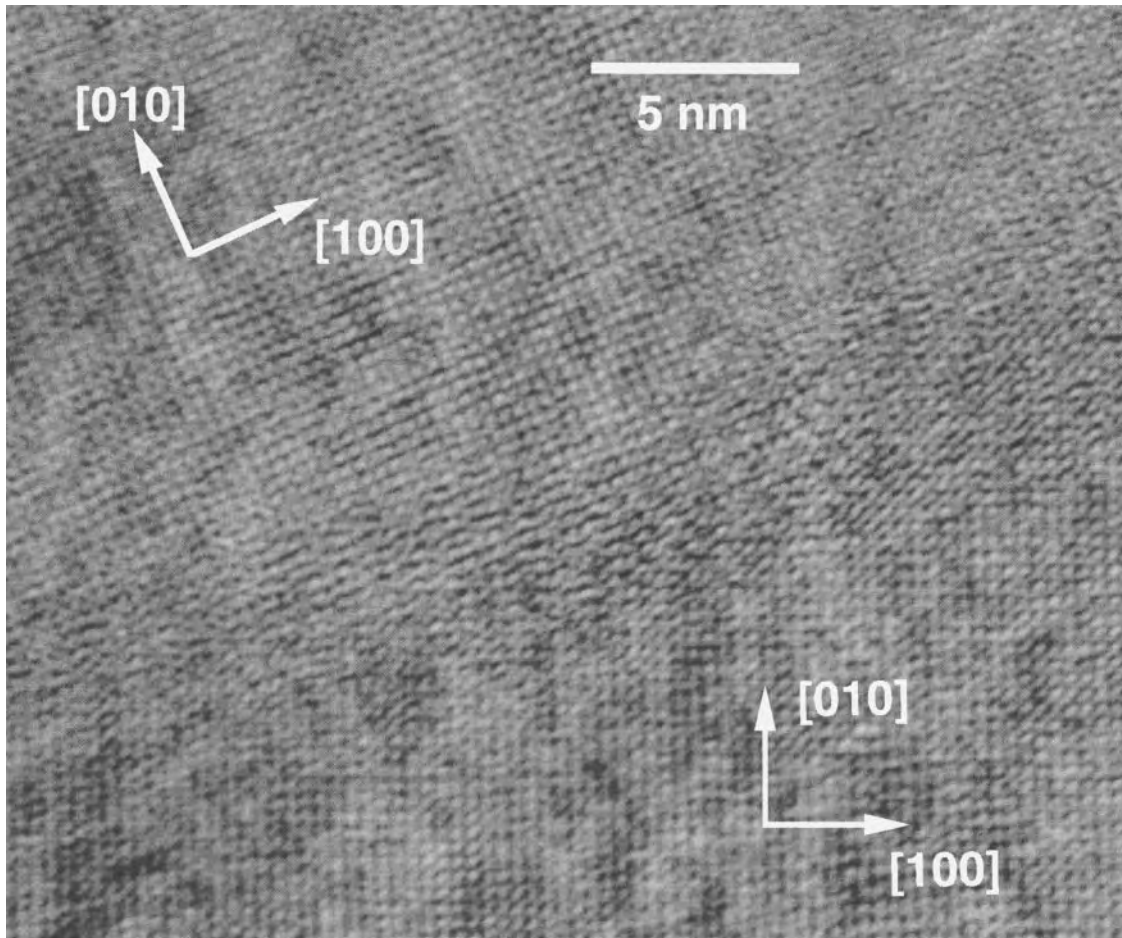


Figure 7. HREM image of a 24° YBCO grain boundary junction grown on a symmetric 24° SrTiO₃ bicrystal template. Note that this area of the boundary is asymmetric which is caused by the macroscopic boundary meandering. The Morie pattern at the boundary indicates an overlap of the two grains. Therefore, the grain boundary is of mixed character, including tilt and twist components.

3. Discussion

As we have shown above, the current distributions for the grain boundary junctions show large scale variations along the length of the boundary. In many incidents there are sizable regions of the grain boundary that carry no current. There have been a number of studies that have indicated that the microstructure at grain boundary junction cores vary extensively [20–27]. Transmission electron microscope studies of grain boundary junctions have shown large variations in the boundary microstructure along the length of the boundary. Boundary precipitates, meandering of the boundary on the order of hundreds of nanometers and faceting on the 10–100 nanometer length scale (the

length and orientation of the facets are dependent on the grain boundary orientation) are dominant features of most grain boundary junctions [20–27]. Meandering is believed to be caused by rapid growth in the a - b plane of the YBCO over the template bicrystal resulting in a YBCO grain boundary junction that does not follow the bicrystal template closely [28]. Studies of symmetric 24° YBCO grain boundaries have indicated that, although the underlying SrTiO₃ substrate is prepared as a symmetric bicrystal, large areas along the boundary are not symmetric due to the boundary meandering [28].

It is evident that the local symmetry at the grain boundary is controlled by the meandering of YBCO across the template bicrystal boundary. Thus the notion

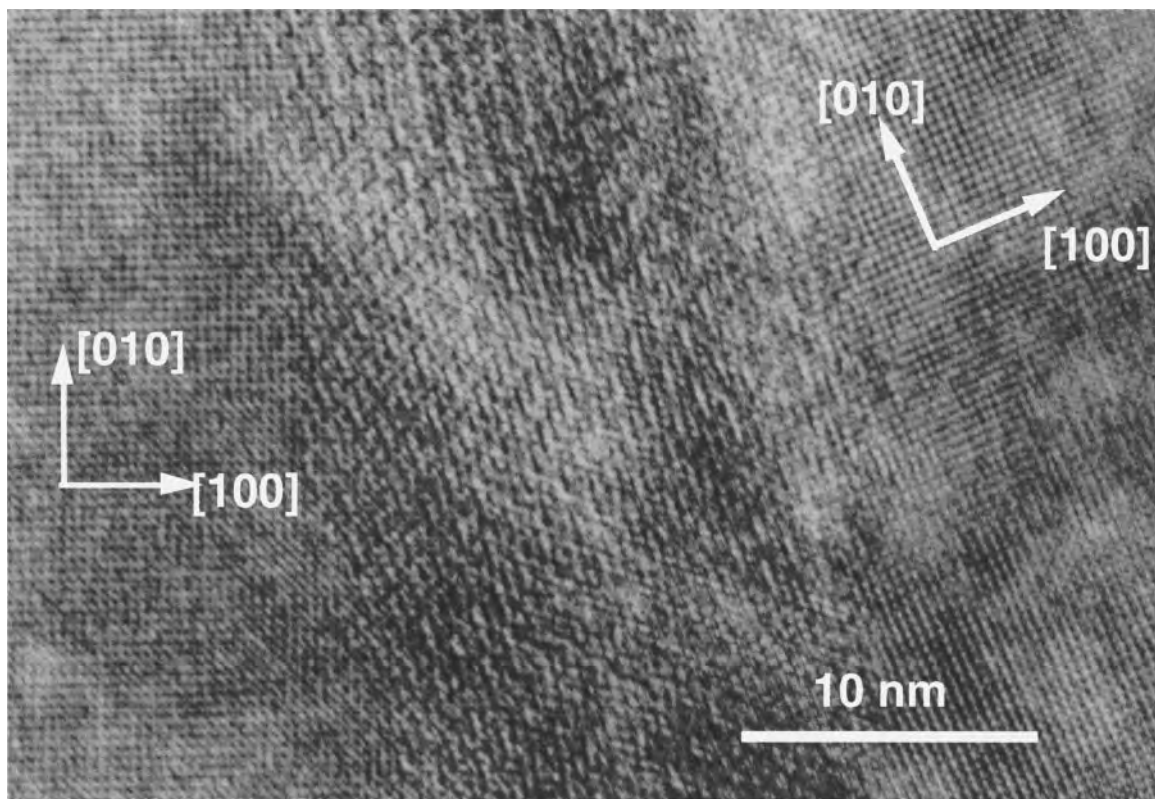


Figure 8. HREM image of a 24° YBCO grain boundary junction. Large Moiré pattern indicates considerable overlapping of the grains.

of distinguishing between symmetric and asymmetric boundaries when discussing the transport properties of grain boundary Josephson junctions is questionable. The nominally symmetric 24° grain boundary junctions used for our analysis show large areas with asymmetric facets. Thus it is important to understand that regardless of the macroscopic symmetry across the grain boundary, no purely symmetric YBCO grain boundary junctions are obtained by the conventional YBCO thin film synthesis techniques. By contrast, Vuchic et al. obtained by a special synthesis technique for 45° grain boundary junctions, [001] YBCO tilt grain boundaries that contained almost exclusively asymmetrical (110)(100) grain boundaries [25]. In this case, although a considerable amount of meandering was present, the grain boundary plane alternated between (110)(100) and (100)(110) facets, which were very well structured. As a consequence relatively high critical currents were obtained for these 45° YBCO grain boundaries.

Clearly, the vast variation in microstructures observed along the length of single grain boundaries, as illustrated in Figs. 6–9, suggest corresponding variations

in the local current carrying capacity of the grain boundary. Structural and chemical disorder, such as amorphous grain boundary phases (Fig. 6) and oxygen depletion severely limit current transport. Whether or not and to what extent grain boundaries that deviate from the tilt configuration (inclined grain boundaries in Figs. 7 and 8) limit supercurrent transport properties is not clear. However, when accompanied with structural disorder, it is expected that the current flow will also be impeded.

Considering the vast variations of the boundary microstructure along the length of a single boundary we conclude that the local structural and chemical variations control the local transport properties across the boundary and result in the current variations along the boundary such as those obtained in Fig. 3. Since the total critical current for a junction (in zero field for example) is dependent on the sum of the local $J(x)$ contributions, it is clear that to maximize the current density of the junction $J_{c,max}$, the local critical currents must be uniform and at their highest possible values. Obviously, this is not the case for a typical grain boundary

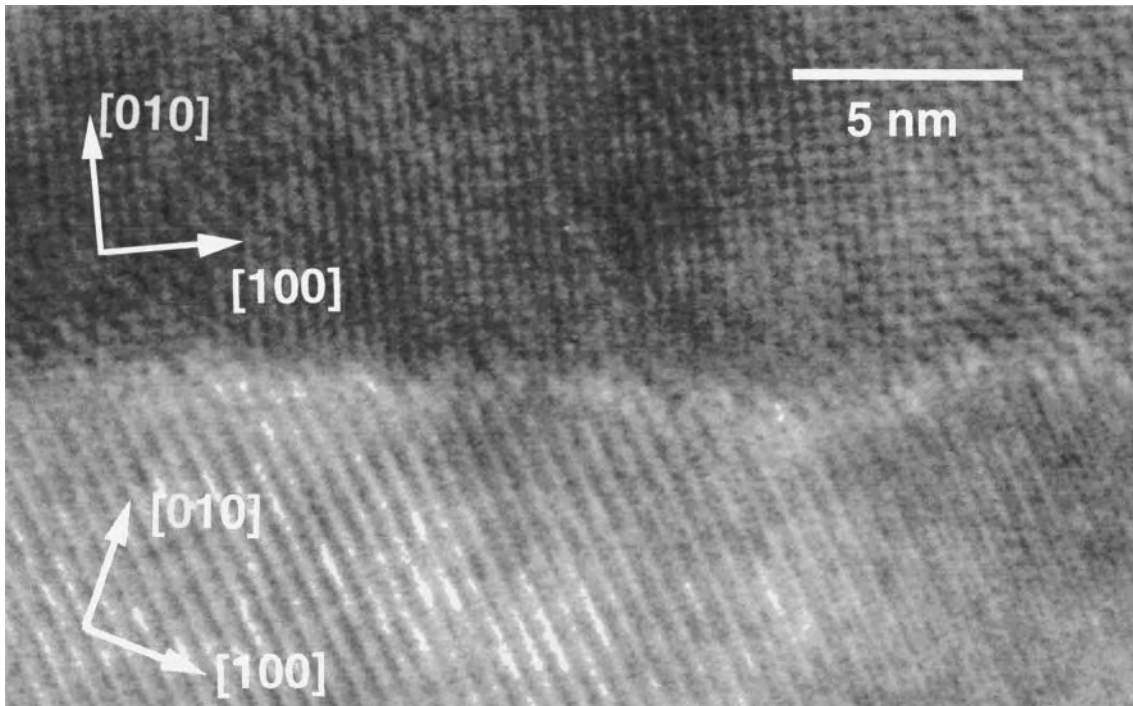


Figure 9. An HREM image of 24° YBCO grain boundary. This section of the boundary is asymmetric. The grains appear to be well connected in this region with no evidence for an amorphous region.

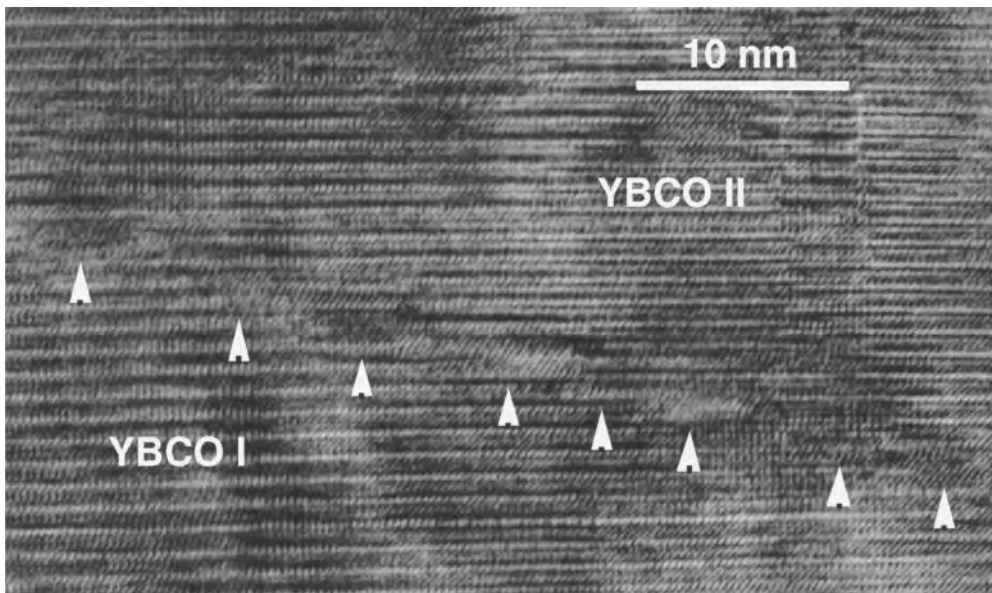


Figure 10. HREM cross-section image of the barrier layer of an interface engineered ramp-edge junction. The barrier layer is thin (2–3 nm), continuous and free of pinholes.

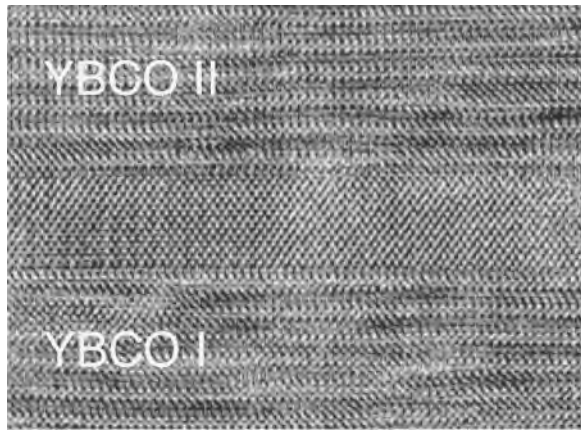


Figure 11. HREM image of a plasma treated barrier grown on the YBCO basal plane. Note the difference in the lattice fringes between the barrier layer and the YBCO layers.

junction. Thus, the great range of critical currents that have been reported in the literature for junctions of the same macroscopic grain boundary geometry can be explained on the basis of differences in the current variations along the grain boundary.

By contrast, the current distributions for the interface engineered junctions from Fig. 5 appear to be highly uniform along the length of the boundary. High resolution electron microscope investigations of the barrier layer has shown that a very uniform layer along the boundary is formed during junction fabrication. The fact that no pinholes or second phases were found is consistent with the uniform current distributions found across the boundaries as noted in Fig. 5.

The direct correlation between a uniform barrier layer and a uniform current distribution highlights the important relationship between the two and thus underscores the notion that future improvements in the transport behavior of all high T_c Josephson junctions must be sought by controlling the quality of the interface region.

Other techniques have been used to gain insight into the current distribution along the length of grain boundary Josephson junctions. Neshet and Ribak attempted to extract the current distribution $J(x)$ along the length of the boundary for grain boundary Josephson junctions using a phase retrieval algorithm [29]. Others have used a correlation function to determine the spacing of the current variations along the boundary [30–34]. Laser scanning microscopy and low temperature scanning electron microscopy have also been employed to estimate the variations of the local current [35–40].

These various techniques have all indicated a complicated current distribution along the length of grain boundary junctions. Measurements of the critical current oscillations at field strengths in the 1–5 Tesla range suggest that the current distribution $J(x)$ along the length of the boundary can vary at subnanometer length scales [30, 33, 41, 42].

Studies of the oxygen stoichiometry along grain boundary junctions have indicated significant variations in the local oxygen content along the length of the boundary [43–45]. These structural and stoichiometric variations along the boundary are all factors contributing to the extreme variations in the current distribution along the length of the grain boundary noted in Fig. 3.

The phase restoration algorithm used to calculate the current distributions $J(x)$ along the length of the boundary is a promising non-destructive technique for obtaining the local current variations along the length of various types of Josephson junctions. The phase retrieval technique assumes a sinusoidal current-phase relation (CPR). Recent work has suggested that the d-wave symmetry nature of the YBCO order parameter may cause deviations from the traditional sinusoidal CPR for certain types of Josephson junctions [46]. Measurements of the CPR performed on 45° YBCO [001]-tilt grain boundaries suggest a deviation from sinusoidal behavior [46]. However, measurements of the CPR for 24° YBCO bicrystal grain boundary junctions and for step-edge junctions similar to the junctions used for our analysis indicate in nearly all cases a sinusoidal current-phase relation [47, 48]. Thus the assumption of a sinusoidal current-phase relation for use in the phase restoration appears to be justified.

4. Summary and Conclusions

A phase retrieval method was used to determine the positional current distribution $J(x)$ along the length of 24° YBCO grain boundary and ramp-edge interface engineered Josephson junctions from experimentally measured critical current vs. applied magnetic flux ($I_c(B)$) measurements. The current distributions along the length of the 24° YBCO bicrystal grain boundary junctions were found to vary extensively from region to region along the boundary. The microstructures of 24° YBCO grain boundary junctions fabricated under identical conditions to the samples used for transport measurements were analyzed by HREM techniques. The microstructure was found to vary extensively from region to region along the length of the boundary.

Meandering of the grain boundary plane controls the local symmetry across the boundary plane and thus can control the structure at the grain boundary cores. HREM analysis indicated grain boundary core regions that were well connected separated by regions along the boundary that were highly disordered. Thus there exists a direct correlation between the variations in the boundary current and the boundary microstructure for grain boundary junctions. In contrast to grain boundary junctions, along the length of ramp-edge interface engineered junctions the current distributions were found to be highly uniform along the length of the junction. HREM analysis of the boundary microstructure indicated that the barrier layer of the interface engineered junctions were uniform, continuous and free of secondary phases or pinholes. A continuous barrier layer of constant thickness is consistent with the uniform current distributions determined by the phase retrieval method for identically fabricated junctions. This provides direct evidence that the uniformity of the current is controlled by the uniformity of the barrier layer and thus future advances in Josephson junction quality and current carrying capacity must address the issue of the uniformity of the boundary microstructure.

Acknowledgments

This work was supported by the National Science Foundation Office of Science and Technology Centers, under contract No. DMR 91-20000 (MC, LDM and YH) and the United States Department of Energy, Basic Energy Sciences-Materials Science, under contract No. W-31-109-ENG-38 (KLM) and National Science Foundation grant No. DMR-9214505.

References

1. E. Olsson and K. Char, *Appl. Phys. Lett.* **64**, 1292 (1994).
2. J.G. Wen, N. Koshuzuka, C. Traehlt, H.W. Zandbergen, E.M.C.M. Reuvekamp, and H. Rogalla, *Physica C* **255**, 293 (1995).
3. Y. Huang, B.H. Moeckly, K.L. Merkle, and K. Char, *Microsc. Microanal.* **4**, 672 (1998).
4. Y. Huang, K.L. Merkle, and K. Char, *Microsc. Microanal.* **3**, 667 (1997).
5. S. Rozeveld, K.L. Merkle, and K. Char, *Physica C* **252**, 384 (1995).
6. D.H. Blank, H.J. Rogalla, *Mater. Res.* **12**, 2953 (1997).
7. B.D. Hunt, M.G. Forrester, J. Talvacchio, and R.M. Young, *Applied Supercond.* **5**, 365 (1998).
8. Ji Ping Zhou and J.T. McDevitt, *Appl. Phys. Lett.* **72**, 848 (1998).
9. L. Antognazza, B.H. Moeckly, T.H. Geballe, and K. Char, *Phys. Rev. B* **52**, 4559 (1995).
10. S. Rozeveld, K.L. Merkle, and K. Char, *J. Mater. Res.* **11**, 281 (1996).
11. K. Char, L. Antognazza, and T.H. Geballe, *Appl. Phys. Lett.* **63**, 2420 (1993).
12. K.L. Merkle, Y. Huang, S. Rozeveld, K. Char, and B.H. Moeckly, *Micron* **30**, 539 (1999).
13. K. Harada, H. Myoren, and Y. Osaka, *Jap. J. Appl. Phys.* **30** L1387 (1991).
14. C.L. Jia, M.I. Faley, U. Poppe, and K. Urban, *Appl. Phys. Lett.* **67**, 3635 (1995).
15. B.H. Moeckly and K. Char, *Appl. Phys. Lett.* **71**, 2526 (1997).
16. B.H. Moeckly, K. Char, Y. Huang, and K.L. Merkle, *Appl. Supercond.* **6**, 317 (1998).
17. M. Carmody, E. Landree, L.D. Marks, and K.L. Merkle, *Physica C* **315**, 145 (1999).
18. M. Carmody, B.H. Moeckly, K.L. Merkle, and L.D. Marks, *J. Appl. Phys.* **87**, 2454 (2000).
19. Y. Huang, K.L. Merkle, B.H. Moeckly, and K. Char, *Physica C* **314**, 36 (1999).
20. J.A. Alarco, E. Olsson, Z.G. Ivanov, P.A. Nilsson, D. Winkler, E.A. Stepantsov, and A.Ya. Tzalenchuk, *Ultramicroscopy* **51**, 239 (1993).
21. C. Traeholt, J.G. Wen, H.W. Zandbergen, Y. Shen, and J.W.M. Hilgenkamp, *Physica C* **230**, 425 (1994).
22. B. Kabius, J.W. Seo, T. Amrein, U. Dahne, A. Scholen, M. Siegel, K. Urban, and L. Schultz, *Physica C* **231**, 123 (1994).
23. J.W. Seo, B. Kabius, U. Dahne, A. Scholen, and K. Urban, *Physica C* **245**, 25 (1995).
24. C.A. Copetti, F. Ruders, B. Oelze, Ch. Buchal, B. Kabius, and J.W. Seo, *Physica C* **253**, 63 (1995).
25. Boris Vuchic, K.L. Merkle, K. Char, D.B. Buchholz, R.P.H. Chang, and L.D. Marks, *J. Mater. Res.* **11**, 75 (1996).
26. X.F. Zhang, D.J. Miller, and J. Talvacchio, *J. Mater. Res.* **11**, 2440 (1996).
27. S. McKernan, M.G. Norton, and C.B. Carter, *J. Mater. Res.* **7**, 1052 (1992).
28. Y. Huang, K.L. Merkle, L.P. Lee, M. Teepe, and K. Char, *Appl. Phys. Lett.* **71**, 3703 (1997).
29. O. Neshet, and E.N. Ribak, *Appl. Phys. Lett.* **71**, 1249 (1997).
30. O.M. Froehlich, H. Schulze, A. Beck, B. Mayer, L. Alff, R. Gross, and R.P. Huebener, *Appl. Phys. Lett.* **66**, 2289 (1995).
31. S. Schuster, R. Gross, B. Mayer, and R.P. Huebener, *Phys. Rev. B* **48**, 16172 (1993).
32. Xu Xiu, Qiang Lu, Shiguang Wang, Yuandong Dai, Guangcheng Xiong, Guijun Lian, Ruijuan Me, Shouzheng Wang, and Zizhao Gan, *Physica C* **282-287**, 2409 (1997).
33. O.M. Froehlich, H. Schulze, A. Beck, R. Gerdemann, B. Mayer, R. Gross, and R.P. Huebener, *IEEE Trans. Applied Superconductivity* **5**, 2188 (1995).
34. L. Alff, B. Mayer, S. Schuster, O. Frohlich, R. Gerdemann, A. Beck, and R. Gross, *J. Appl. Phys.* **75**, 1843 (1994).
35. Y.Y. Divin, H. Schulz, U. Poppe, N. Klein, K. Urban, P.M. Shadrin, I.M. Kotelyanski, and E.A. Stepantsov, *Physica C* **256**, 149 (1996).
36. P.M. Shadrin and Y.Y. Divin, *Physica C* **297**, 69 (1998).
37. R. Gerdemann, K.D. Husemann, R. Gross, L. Alff, A. Beck, B. Elia, W. Reuter, and M. Siegel, *J. Appl. Phys.* **76**, 8005 (1994).
38. G.M. Fisher, B. Mayer, R. Gross, T. Nissel, K.-D. Husemann,

- R.P. Huebener, T. Freltoft, Y. Shen, and P. Vase, *Science* **263**, 1112 (1994).
39. J. Mannhart, R. Gross, R.P. Huebener, P. Chaudhari, D. Dimos, and C.C. Tsuei, *Cryogenics* **30**, 397 (1990).
40. A. Marx, K.D. Husemann, B. Mayer, T. Nissel, R. Gross, M.A.J. Verhoeven, and G.J. Gerritsma, *Appl. Phys. Lett.* **64**, 241 (1994).
41. E. Sarnelli, P. Chaudhari, and J. Lacey, *Appl. Phys. Lett.* **62**, 777 (1993).
42. M. Daumling, E. Sarnelli, P. Chaudhari, A. Gupta, and J. Lacey, *Appl. Phys. Lett.* **61**, 1355 (1992).
43. S.E. Babcock and D.C. Larbalestier, *Appl. Phys. Lett.* **55**, 393 (1989).
44. V.P. Dravid, H. Zhang, and Y.Y. Wang, *Physica C* **213**, 353 (1993).
45. B.H. Moeckly, D.K. Lathrop, and R.A. Buhrman, *Phys. Rev. B* **47**, 400 (1993).
46. E. Il'ichev, V. Zakosarenko, R.P.J. Ijsselsteijn, V. Schultze, H.G. Meyer, H.E. Hoenig, H. Hilgenkamp, and J. Mannhart, *Phys. Rev. Lett.* **81**, 894 (1998).
47. Polushkin, S. Uchaikin, S. Knappe, H. Kock, B. David, and D. Grundler, *IEEE Trans. Appl. Supercond.* **5**, 2790 (1995).
48. V. Zakosarenko, E.V. Il'ichev, R.P.J. Ijsselsteijn, and V. Schultze, *IEEE Trans. Appl. Supercond.* **7**, 1057 (1997).